The role of the heating mode of the mantle in intermittent reorganization of the plate velocity field

Julian P. Lowman,[1] Scott D. King[2] and Carl W. Gable[3]

[1]*School of Earth Sciences, University of Leeds, Leeds, West Yorkshire LS2 9JT, UK. E-mail: J.Lowman@earth.leeds.ac.uk*
[2]*Department of Earth and Atmospheric Sciences, Purdue University, West Lafayette, IN 47907-1397, USA. E-mail: sking@purdue.edu*
[3]*Hydrology, Geochemistry and Geology Group (EES-6), Los Alamos National Laboratory, MS T003, Los Alamos, NM 87545, USA. E-mail: gable@lanl.gov*

SUMMARY

The geological record indicates that stages of relatively steady plate motion have been punctuated by comparatively brief periods in which plate velocities have reorganized. The distribution of buoyancy sources in the mantle has generally been regarded as evolving too slowly to explain these rapid transitions in plate velocity. We investigate the feedback between mantle convection and plate velocity using 2-D and 3-D mantle convection models that incorporate mobile dynamic plates. We focus on the influence of internal heating in the mantle and consider the effect of mantle viscosity stratification and different plate geometries on the plate velocity time dependence. As either the Rayleigh number or the internal heating rate is increased to magnitudes approaching mantle values, the record of the plate motion from our calculations becomes characterized by intermittent changes in direction. This behaviour is a result of the influence of plates on heat loss from the inherently unsteady, internally heated convecting system. Plate motion instills a pattern of organization on the underlying convection that reflects the plate geometry and results in the formation of sheet-like downwelling structures at convergent plate boundaries in both 2-D and 3-D calculations (in contrast, upwellings in 3-D models are not sheet-like). The role of the sheet-like downwellings is critical in the observed episodic reorganization of the plate velocities. Warm material below the plates is entrained by plate motion into regions enveloping the downwelling sheets. During periods of fairly steady plate motion, buoyancy associated with the build-up of heat around the downwelling sheets leads to the creation of an unstable convection pattern. This build-up of heat is dramatic in calculations with mantle-like internal heating rates and resists continued long-term plate motion towards mature downwellings. When there are limitations on the degree of freedom of the direction of plate movement, such as in 2-D models, these effects even more pronounced. Accordingly, the effect of plates on mean global thermal quantities is more dramatic in 2-D calculations than it is in 3-D calculations. Nevertheless, 3-D calculations incorporating plates of different sizes do exhibit rapid reorganizations in their convection patterns as the pull of young slab-like features supersedes the pull of mature downwelling sheets. We compare the timing and frequency of the reorganization events in our calculations with the general characteristics of plate motions determined from plate reconstruction studies.

Key words: fluid dynamics, heat flow, instability, mantle convection, plate tectonics.

1 INTRODUCTION

While important strides are being made in producing mantle convection models with nearly rigid plates and concentrated zones of plate boundary deformation, an important feature of plate history that has not been emulated in mantle convection calculations are the periods of stable plate velocity (stages) separated by comparatively brief episodes of plate velocity reorganization (stage transitions).

The sharp bend in the Hawaii–Emperor seamount chain at 43 Ma is perhaps the best known indication that plates can undergo rapid changes in direction (e.g. Engebretson *et al.* 1985; Stock & Molnar 1987). The erupted basalts associated with the seamounts that delineate the path of the Pacific plate relative to the Hawaiian hotspot indicate that the plate changed direction by approximately 60°—from almost northward-moving, to its present-day northwesterly path (e.g. Clague & Dalrymple 1987). Moreover, the timing of the basalt

eruptions suggests that the change in direction occurred over less than 3×10^6 yr (Clague & Dalrymple 1987). While the change in direction of the Pacific plate is widely accepted, the fundamental cause of the change in motion is not well understood. Suggestions that there may be a link in the close temporal spacing between the India–Asia collision (e.g. Patriat & Achache 1984; Clague & Dalrymple 1987) and the change in direction of the Pacific plate do not appear to have dynamic support (Richards & Lithgow-Bertelloni 1996). Alternative theories invoking changes in plate boundary forces (such as the initiation of new Western Pacific subduction zones, Gordon *et al.* 1978) may provide more plausible explanations for the driving mechanism that causes a change in plate velocity.

Subduction along the Izu–Bonin–Mariana island arc system has been inferred based on widespread magmatism in the associated island arc system as early as 48 Ma (Stern & Bloomer 1992). One possibility is that this emerging subduction zone affected the force balance on the Pacific plate as the nascent slab began pulling the plate in a westerly direction. If this was the case, then it is unclear why motion towards mature subduction zones did not continue to control the associated plate motion. The origin of the force responsible for the compression that initiated subduction along a new or previously conservative (transform) boundary also remains unidentified. Furthermore, it is not clear that subduction initiation could generate the required buoyancy to offset plate motion in less than 5 Myr. Indeed, because changes in plate direction appear to occur relatively rapidly (over ∼3 Myr in the case of the Pacific plate), it has been argued that because of the long timescales associated with mantle convection processes, changes in plate direction must result from tectonic forces rather than the evolution of the buoyancy field of the mantle. To test this hypothesis, we have investigated the feedback between plate velocity and mantle convection by examining a variety of mantle convection calculations incorporating plates with dynamically evolving velocities. The problem requires both a 3-D geometry and sufficient resolution to model vigorous mantle convection.

The planform and evolution of flow in the mantle are largely controlled by the geometry of the surface plates (e.g. Parmentier & Turcotte 1978; Lux *et al.* 1979; Davies *et al.* 1988, 1989; Gurnis & Zhong 1991; Bunge & Richards 1996; Zhong *et al.* 2000; Lowman *et al.* 2001; Monnereau & Quéré 2001), the viscosity stratification (Gurnis & Davies 1986; Hansen *et al.* 1993; Bunge *et al.* 1996, 1997) and the ratio of basal to internal heating (e.g. McKenzie *et al.* 1974). Each of these influences affects the convective wavelength and, consequently, the heat flow and mean temperature of the convecting medium. This indicates that in order to understand how mantle convection affects plate motion, it is necessary to incorporate dynamic plates in the calculations (that is, plates that change velocity in response to the evolving buoyancy distribution within the mantle).

There are at least two philosophies concerning the inclusion of dynamic plates in numerical mantle convection experiments. The simpler approach invokes the existence of plates explicitly. Examples of such approaches include specifying plate-like surface motion as a time-dependent boundary condition that responds to the flow evolution (Gable *et al.* 1991; Monnereau & Quéré 2001) or specifying static rheologies conducive to inducing plate-like surface motion in stiff zones separated by weak plate boundaries (Gurnis 1989; King & Hager 1990). Both methods include plate–mantle feedback so that plate motion is determined by mantle buoyancy forces. However, plate boundary evolution is not accounted for in these types of models.

Alternatively, it may be possible to include rheology in the convecting system that allows for plate-like behaviour to evolve self-consistently (e.g. Tackley 1998, 2000; Trompert & Hansen 1998). While this approach offers the hope of insight into the self-generation of plate motion and the underlying dynamics associated with the growth of new plate boundaries, it is not required for studying the long-term coupling between plates and mantle convection. Indeed, in contrast to the former methods, the computational demands of self-consistent plate generation models mean they have not yet reached the maturity required for studying mantle convection with thermal boundary layers that scale to the thickness of the Earth's lithosphere. In order for the effects of long-term coupling of plates and mantle convection to become manifest such systems need to be studied over periods that scale to hundreds of millions of years. Our findings indicate that the most critical element in studying the evolution of plate velocities is the requirement of modelling convection over long integration times with Earth-like heating parameters.

The presence of internal heat sources (whether representative of radiogenic heating of the mantle or secular cooling) influences the wavelength and time dependence of convection. In the range of convective vigour characterizing convection in the mantle, isoviscous, internally heated convection below either rigid or free-slip boundaries is highly time dependent and exhibits flow patterns of a much shorter wavelength than basally heated convection with corresponding boundary conditions (e.g. McKenzie *et al.* 1974; Jarvis 1984; Parmentier *et al.* 1994; Sotin & Labrosse 1999). In addition, if the internal heating rate is held fixed, increasing the Rayleigh number of an isoviscous fluid heated by both a constant temperature boundary condition and internal sources decreases the mean temperature of the fluid (e.g. Sotin & Labrosse 1999). Thus, in contrast to entirely basally heated convection, the mean temperature of an internally heated fluid is a strong function of the Rayleigh number. Moreover, the temperature structure of an internally heated, convecting fluid is quite different from the structure observed in lower Rayleigh number calculations. The temperature structure between 2-D and 3-D internally heated convection calculations also differs. In 2-D, internally heated convection is characterized by weak, diffuse, upwelling and vigorous, focused, downwelling sheets. The result of the asymmetry in the vigour of the upwellings and downwellings is that the centre of circulation of the convection cells is shifted toward the sinking material. The cells (or 'rolls') of internally heated, 2-D convection become increasingly asymmetric as either the internal heating rate or Rayleigh number are increased (Jarvis & Peltier 1982). The contrast in vigour between upwellings and downwellings in 3-D Cartesian geometry studies is similar to that observed in 2-D studies; however, unlike the sheet-like features in 2-D calculations, the upwellings and downwellings in internally heated, 3-D Cartesian geometry studies are plume-like (e.g. Houseman 1988; Travis *et al.* 1990; Parmentier *et al.* 1994; Sotin & Labrosse 1999).

The study described here includes both 2-D and 3-D calculations of vigorous mantle convection. The work was motivated by a 2-D study of highly time-dependent, internally heated convection calculations incorporating dynamic plates presented by Lowman *et al.* (2001). This work identified cyclic patterns in the dynamic plate velocities exhibited by their calculations and showed that this behaviour is robust in calculations with a wide range of aspect ratios, multiple plates, and both reflecting and wraparound sidewall boundary conditions. However, the 2-D models explored in that study covered a limited range of heating rates and Rayleigh numbers. It is the goal of this work to determine what heating conditions are necessary

for the appearance of the flow reversal behaviour and whether this behaviour is exhibited in 3-D geometry.

The approach of our investigation is guided by the computational restrictions of exploring a parameter range requiring high-resolution calculations. Using the 2-D calculations we identify the extent of the parameter space where time-dependent convection results in dramatic changes in plate velocity (Lowman *et al.* 2001). We then explore a manageable number of the highest Rayleigh number 3-D calculations possible, allowing for adequate numerical resolution, within the parameter space identified by the 2-D study.

Having already extensively studied the robustness of flow reversal behaviour in different aspect ratio 2-D calculations for Earth-like Rayleigh numbers (Lowman *et al.* 2001) we let the limits on the size of the 3-D computational domain dictate the aspect ratio of the 2-D models that will be used to constrain the 3-D study. A $2 \times 2 \times 1$ solution domain requires approximately 6×10^6 nodes in order to resolve calculations with the Rayleigh numbers we wish to investigate here. Examining a suite of 3-D calculations with larger aspect ratios is presently an untenable project. Consequently, given the knowledge that the time dependence described in our 2-D results has been observed over a wide variety of different aspect ratio calculations, in this study we have chosen to examine models with an aspect ratio of 2 exclusively, this enables a systematic and straightforward comparison of 2-D and 3-D results. However, we must recognize that, as with all such studies, model behaviour may be influenced by the limitation of the aspect ratio used for the study.

We initially investigate the effect of the heating mode on convection patterns in 60 2-D calculations with two types of surface boundary conditions and two viscosity structures. In all calculations we specify an isothermal, basal boundary condition. The heating mode is dictated by a pair of independent parameters, a Bénard–Rayleigh number and an internal heating rate (e.g. Weinstein *et al.* 1989; Travis *et al.* 1990; Travis & Olson 1994; Sotin & Labrosse 1999).

2 MODEL DESCRIPTION

We consider thermal convection at infinite Prandtl number in an incompressible, Boussinesq fluid and specify a Cartesian geometry. A Newtonian, depth-dependent viscosity is assumed and we allow for the inclusion of uniformly distributed internal heat sources. The governing equations for the evolution of the fluid are taken from the conservation of mass, momentum and energy and take the form

$$\nabla \cdot \mathbf{v} = 0, \tag{1}$$

$$\nabla \cdot [\eta(z)\dot{\epsilon}] - \nabla P = Ra_\text{B} T \hat{\mathbf{z}}, \tag{2}$$

and

$$\frac{\partial T}{\partial t} = \nabla^2 T - \mathbf{v} \cdot \nabla T + \frac{Ra_\text{H}}{Ra_\text{B}}, \tag{3}$$

respectively. The non-dimensional quantities in the equations above are: $\mathbf{v}$, velocity; $\eta(z)$, depth-dependent dynamic viscosity; $\dot{\epsilon}$, the strain rate tensor; P, pressure; T, temperature; and t, time. Ra_B is the Bénard–Rayleigh number (Chandrasekhar 1961) and is given by

$$Ra_\text{B} = \frac{g\alpha\Delta T d^3}{\kappa\nu}, \tag{4}$$

where g is gravitational acceleration; α is the thermal expansivity; ΔT is the superadiabatic temperature difference between the top and bottom boundaries; d is the depth of the convecting layer; κ is the thermal diffusivity and ν is the kinematic viscosity.

The convecting layer is confined between isothermal horizontal boundaries in all calculations. The internal heating rate is specified by the ratio $H = Ra_\text{H}/Ra_\text{B}$ where

$$Ra_\text{H} = \frac{g\alpha\varepsilon d^5}{\kappa k\nu}, \tag{5}$$

and ε is the rate of internal heat generation per unit volume.

A hybrid spectral finite-difference scheme, previously described by Gable *et al.* (1991) for 3-D convection, has been used to solve the system of equations (1)–(3). The code has been benchmarked for a variety of problems that do not include plates and shows excellent agreement with the results obtained from other numerical methods in those cases (e.g. Travis *et al.* 1991; Busse *et al.* 1993).

Plates are modelled by specifying a finite-thickness viscous layer at the top of the calculations and prescribing piecewise uniform surface velocities. The viscosity of the plates is 1000 times greater than the reference viscosity used in the definition of the Rayleigh numbers. The plates are passive and neither drive nor resist the convective flow. This condition is achieved by continually updating the plate velocities so that the integrated shear stresses on the base of a plate vanish at all times. Thus, plate velocities evolve to reflect the distribution of buoyancy within the plate and the underlying fluid. The resulting condition is consistent with a rigid plate distributing the applied stresses. The plate geometry remains unchanged during each calculation. The high-viscosity layer at the top of the domain acts as a first-order approximation for the stiffness associated with the Earth's cold lithosphere. Below this layer we specify either a viscosity that increases with depth or a uniform viscosity. For all calculations, the plates have a non-dimensional thickness of approximately $0.05d$ (a thickness representative of the mean thermal boundary layer thickness of the higher Rayleigh number calculations that we have examined). The plate calculation has been compared with material methods and power-law rheology plate generation methods and the agreement between the surface heat flux and plate velocities of these calculations was found to be excellent (King *et al.* 1992).

We examine both isoviscous and depth-dependent viscosity calculations. The depth-dependent viscosity specified in the non-isoviscous calculations is based on the general trend derived from joint inversions of post-glacial sea level histories and long-wavelength, convectively supported, free-air gravity harmonics (Forte & Mitrovica 1996). We use a fit for the radial viscosity profile that was determined by Pysklywec & Mitrovica (1997). The viscosity model used is characterized by a factor of 36 increase in viscosity with depth, with the highest gradient occurring in a depth range of 700–1200 km. The viscosity employed in the determination of the Rayleigh numbers quoted in the remainder of the paper has a non-dimensional value of 1.0. Thus, Rayleigh numbers based on the highest viscosity in our stratified viscosity models would be a factor of 36 smaller than those quoted in the text.

Subduction of cool sheet-like downwellings (slabs) is included in our models explicitly. Mass conservation results in the cooled upper thermal boundary layer material carried in the mechanical plates being forced into the mantle along convergent plate boundaries. The result is a typically sheet-like feature, which is anomalously cold like a descending slab. However, the disregard of temperature-dependent viscosity in our models means that the cool, stiff, upper thermal boundary layer material (plate) that plunges into the mantle at convergent plate boundaries is a negatively buoyant but weak feature. (The viscosity of the subducted material takes on the ambient depth-dependent value.) Thus, in our models, the sheet-like downwellings that develop at convergent boundaries are analogous

to subducted plates in their thermal structure but are more easily deformed than high-viscosity slabs.

3 RESULTS

3.1 2-D Results

The observed convective wavelength and the character of the time dependence in 60 2-D experiments are summarized in Fig. 1. Half-black/half-white symbols are used in Fig. 1 to indicate calculations where plates were observed to intermittently reverse direction. Calculations where the time-series of plate velocity magnitude features a single local maximum between plate reversals (the plate velocity magnitude reaches zero at the instant of reversal) are indicated by symbols with a checked pattern. The juxtaposition of the plots in the figure indicates that the onset of periodic flow reversal behaviour in isoviscous calculations with plates correlates with the observation of a change of free-slip surface convection calculations with the same heating modes from two cell flows into multicell, time-dependent flows. (We classify the number of convection cells based on the typical number of distinct upwellings present in the system: three upwellings are therefore interpreted as six cells.) Although

a correlation between multicell, free-slip flow and plate reversals is not indicated in the depth-dependent viscosity calculations, it is clear that changing heating mode causes similar transitions in the time-dependent behaviour of both isoviscous and depth-dependent viscosity calculations with plates. In fact, we observe that for depth-dependent viscosity calculations, flow reversals are manifested in the same $Ra_B - H$ parameter range where regular upper thermal boundary layer instabilities are observed in free-slip surface convection calculations.

Fig. 1 indicates that all of the calculations that include a pair of plates are characterized by a pair of roughly unit aspect ratio convection cells. At lower values of Ra_B, calculations with plates evolve into steady-state flows for both isoviscous and depth-dependent viscosity, however, as the Rayleigh number and internal heating rate are increased, the flows become time-dependent. As Ra_B and H are increased further, each convection cell exhibits a time-dependent behaviour characterized by complete reversals in the sense of the motion of the convective flow (i.e. from clockwise 2-D flow to counterclockwise flow). Accordingly, the plate velocity, which responds to the buoyancy distribution in the flow, reverses direction. These reversals become more frequent and periodic as the Rayleigh number and the internal heating rate approach values thought to characterize
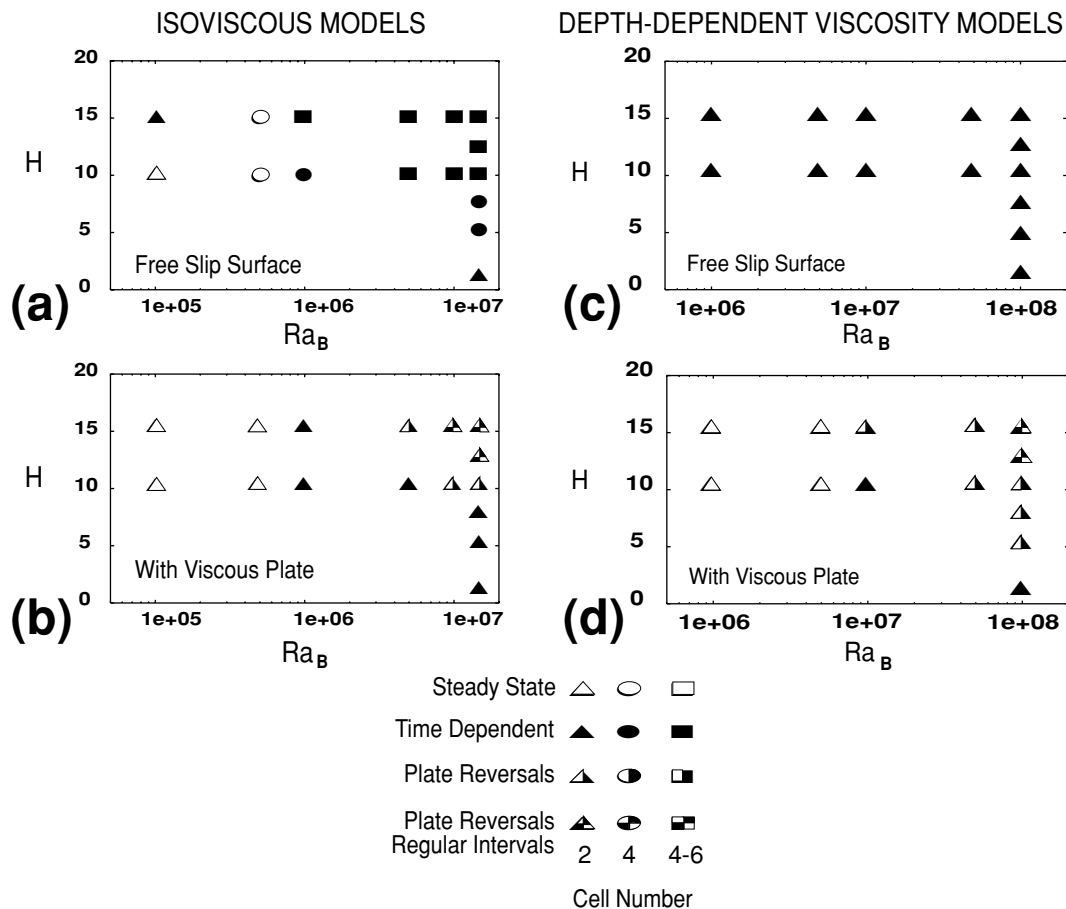
Figure 1. Classification of convection character as a function of Bénard–Rayleigh number, Ra_B, and internal heating rate, H. All of the calculations examined calculations with an aspect ratio of 2 with wrap around sidewalls (periodic boundary conditions). The calculations including plates incorporate a pair of unit width plates with a thickness of $0.052d$. Bénard–Rayleigh numbers are defined with reference to a non-dimensional viscosity of 1.0. In models without plates this is the non-dimensional viscosity at the surface of the model. In the models that include plates, the non-dimensional surface viscosity has a value of 1000 (the plate viscosity) and the viscosity at the base of the plates is 1.1. Symbols are defined in the key and indicate degrees of time dependence and the average number of convection cells present in 2-D aspect ratio two calculations. Calculations are performed with either a uniform viscosity or a viscosity that increases with depth (described in text). Calculations with viscous plates include a pair of unit width plates of thickness $0.052d$.
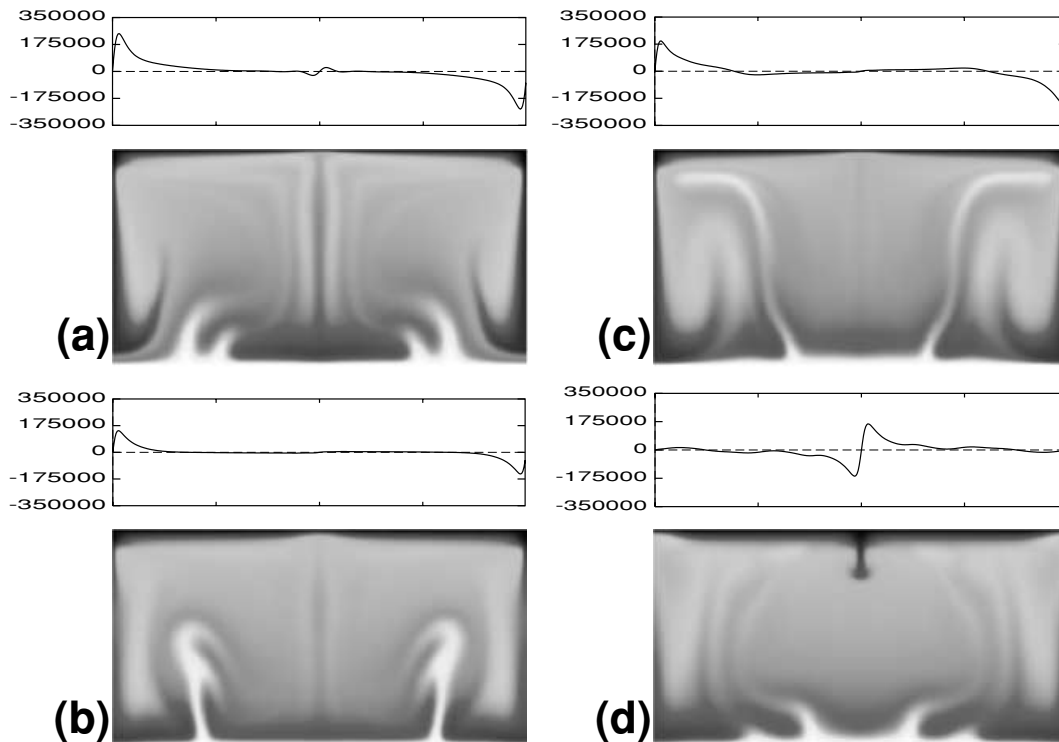
Figure 2. Sequence of temperature field plots from a 2-D model with an aspect ratio of 2 incorporating a pair of equal size (unit width) plates. The plates have a thickness of $0.052d$ and a viscosity that is 1000 greater than the fluid immediately below. The viscosity below the plates increases with depth. The Bénard–Rayleigh number, Ra_B, is 5×10^7 and the internal heating rate, H, is 15. Above each temperature field plot is a profile of the non-dimensional shear stress (τ_{xz}) at the base of the plates resulting from the instantaneous buoyancy distribution within the fluid (i.e. the shear stress in the absence of plate motion). The fields are shown at intervals of 0.0005.

the mantle (e.g. for isoviscous convection, $Ra_H/Ra_B \sim 15$, $Ra_B \sim 10^7$). Such behaviour was described previously by Lowman *et al.* (2001).

Fig. 2 shows a sequence of temperature field snapshots from a depth-dependent viscosity calculation incorporating a pair of plates and illustrates a typical flow reversal sequence in a calculation where Ra_B is 5×10^7 and $H = 15$. This heating mode, geometry and viscosity structure determine that roughly 60 per cent of the surface heat flux from this calculation is caused by internal heating. Shown above each temperature field is a plot of the shear stress, owing to buoyancy alone (i.e. in the absence of plate motion), acting on the base of the viscous plate.

The sequence of temperature fields depicted has been taken from a calculation that has run for 0.04 time units. The frames in the figure are output at intervals of 0.0005. The initial temperature field was random and non-symmetric. The influence of the plate geometry, which is symmetric about the vertical mid-plane of the frames, is clearly apparent in the temperature field. However, the symmetry is not mathematically enforced on the temperature field, it occurs as a result of the feedback between the symmetric plate geometry and convection over a long integration time.

In Fig. 2(a), following a plate flow reversal, half of the same downwelling is seen descending at each side of the temperature field plot. The shear stress plotted above the temperature field shows that there is a strong pull on the base of the plates toward the downwelling limb. In Fig. 2(b) the initial vigour of the downwelling has waned and the upper thermal boundary layer has thickened slightly, reflecting a decrease in the plate velocity. During this period, the shear stress on

the base of the plates is dominated by the flow of the upper mantle toward the cold downwelling. Fig. 2(c) shows that hot material originating from both internal heat sources and active upwellings does not reach the surface of the system. The thick viscous plate acts as a physical barrier to the upwelling flow and also shears the upwelling material in the shallow mantle as a result of its motion. Heat trapped below the plate is dragged by plate motion toward the downwelling flow where, owing to its buoyancy, the warm subplate material resists being pulled deep into the mantle. Consequently, the sources of buoyancy gather around the downwelling sheet and oppose the pull of the plate toward the downwelling flow. As the plate motion slows, the source of cold material supplied to the convergent margin is reduced and the buoyancy of the warm material overcomes the downward drag of the cold downwelling. The flow reverses (Fig. 2d) and a new downwelling forms at what had been the divergent plate margin, reversing the large-scale flow.

A similar result was described previously by Lowman *et al.* (2001) for high Rayleigh number isoviscous calculations with and without a component of basal heating. However, flow reversals are not observed in any of our calculations until some critical internal heating rate has been reached. The presence of internal heating is a critical element in creating the unstable situation that leads to flow reorganization. In a system made inherently unstable by internal heating, the contribution of heat from active upwellings may add a component of time dependence that contributes to triggering the onset of the flow reorganization process. However, the buoyancy of these upwellings is relatively small compared with the gathered accumulated buoyancy of the internal heat sources.
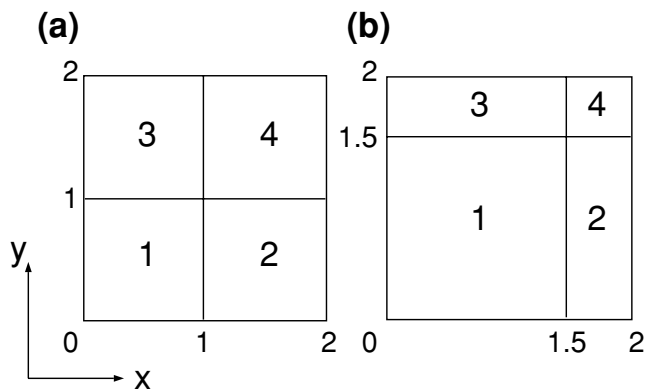
Figure 3. Planforms of the plate geometries employed in the 3-D calculations. The plate numbering sequence is with respect to the coordinate system indicated and corresponds to subsequent figures and to discussion in the text.

3.2 3-D Results

We now examine several 3-D calculations with Rayleigh numbers in the range associated with flow reversals in the 2-D calculations. The purpose is to determine whether flow reversals are manifested in systems where plates are free to move in any direction (rather than just two directions, as is the case in a 2-D calculation) and whether there are any fundamental differences in the global thermal statistics of the 3-D plate calculations in comparison with their 2-D counterparts.

Based on the results of the 2-D calculation study we have determined that the 3-D isoviscous calculations should have a Rayleigh number, Ra_B, of at least 5×10^6 and a heating rate, H, of 15. At this heating mode, time-dependent behaviour in the 2-D calculations with plates was distinguished by *intermittent* plate reversals. Although regular flow reversals were observed in even more vigorously convecting calculations we cannot feasibly compute such a high Rayleigh number flow in a suite of 3-D calculations given our present resources. However, we are able to calculate 3-D flow in both the isoviscous and depth-dependent viscosity cases at heating modes where at least some flow reversals were observed in the 2-D cases. The resolution of the 3-D calculations is $216 \times 216 \times 128 = 5\,971\,968$ grid cells in a $2 \times 2 \times 1$ solution domain.

We first consider the case of a plate geometry with four square 1×1 plates: a geometry that is consistent with the unit-width plates in the 2-D calculations. (This particular geometry will allow for the 3-D calculation to mimic the 2-D calculations exactly but also provides unlimited freedom for flow to evolve with velocities that have a component in 3-D.) To conclude the study, we will examine non-symmetric plate geometries. The 3-D calculation plate geometries are illustrated in Fig. 3.

In Fig. 4 we present a sequence from an isoviscous calculation that includes four square plates. We refer to this calculation as model 3D1 in the text below. Similarly to a 2-D model, this calculation is characterized by cold, downwelling sheets that form at convergent plate boundaries; however, rather than hot rising sheets, 3-D plume-like features are now present in the flow. The sequence shown depicts the evolution of the temperature field of model 3D1 during a flow reorganization event that is driven by a similar source to the buoyant regions that produced the flow reversals in the 2-D calculations. Using arrows superimposed on a diagram of the plate geometry, Fig. 4 also shows the instantaneous plate velocities corresponding to each temperature field. The arrow lengths are proportional to the
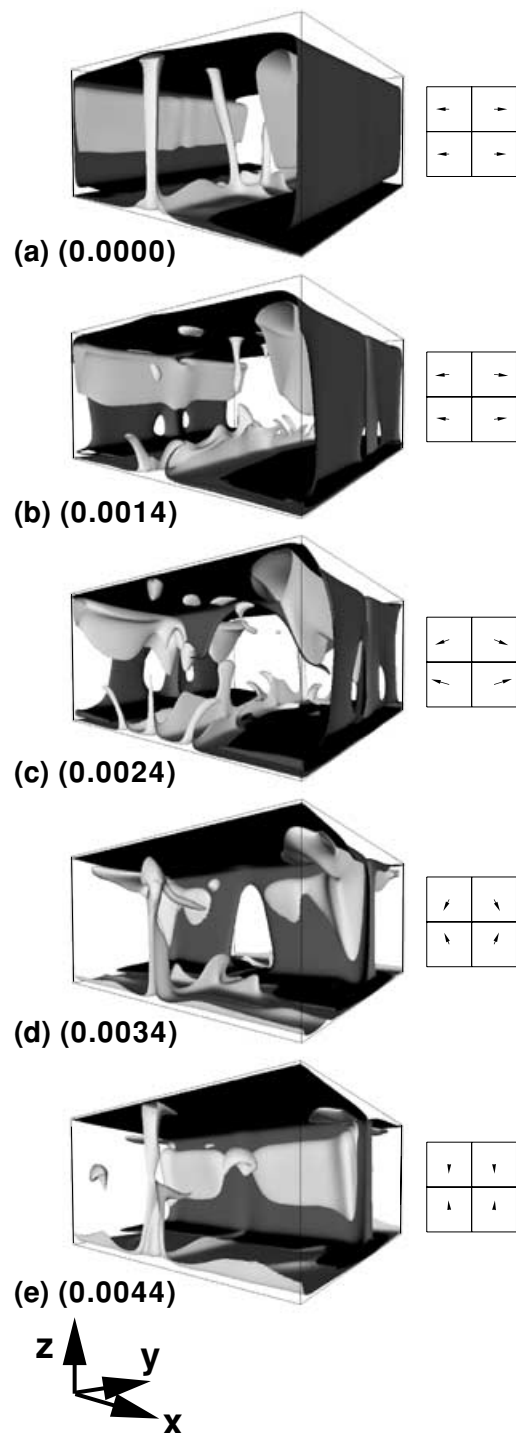
Figure 4. Model 3D1: sequence of temperature field isosurfaces from a 3-D calculation in a $2 \times 2 \times 1$ geometry with four equal size square plates (each 1×1). Each temperature field plot is accompanied by a figure of the plate geometry for the calculation showing the corresponding plate velocity direction. The plate velocity magnitude is indicated by the arrow length. The calculation Rayleigh number, Ra_B, is 5×10^6, the rate of internal heating is 15. The plates have a thickness of $0.052d$ and a viscosity that is 1000 times greater than the isoviscous fluid below. The time that has elapsed between frame (a) and each subsequent frame is indicated in parentheses next to each plot. The light coloured isosurface corresponds to a temperature, T, of 0.91. The dark isosurface corresponds to a temperature of 0.71. The mean temperature from the calculation is 0.81. The calculation resolution is $216 \times 216 \times 128$.

plate velocity magnitude. In this calculation, each plate changes direction in stages characterized by approximately 90° rotations.

As was observed in the 2-D calculations, the presence of the plates in the 3-D calculations instills a wavelength on the convection that reflects the dimensions of the plate geometry. By affecting the characteristic wavelength of the system, the plates affect the ability of the convection to efficiently rid the layer of heat and the mean temperature of the fluid becomes considerably greater than in a free-slip convection calculation. The sequence of panels in Fig. 4 show that, as was observed in the 2-D calculations, hot parcels of fluid have built-up in the 3-D calculation and envelop the cold descending sheets that sink at convergent plate boundaries. In addition to controlling the convection cell wavelength, the plates are a physical barrier to vertical flow and the high plate viscosity suppresses the formation of instabilities within the upper thermal boundary layer. As in the 2-D calculations that exhibited flow reversals, in model 3D1 buoyancy builds in the region around the downwelling sheet and the plate velocity responds by changing direction. The result is that a new convergent boundary develops along one of the transform plate boundaries that runs perpendicular to the initial convergent plate boundary. The 90° angles in the specified plate geometries are conducive to 90° changes in plate motion. As material starts to sink along the new convergent boundary, the plate rotates so that the motion becomes perpendicular to both the new convergent plate boundary and a corresponding new divergent plate boundary. Previously, each of these boundaries had been dominated by strike-slip motion. At the end of the sequence shown in Fig. 4, the initial convergent and divergent boundaries are predominantly strike-slip.

Fig. 5 is a plot of the time-series of the magnitude of the plate velocities for model 3D1. Times corresponding to panels (a) and (e) of Fig. 4 are indicated. The directions of plate motion of each of

the corresponding plates are also indicated in the figure by uniform length arrows in the plane of the page. The *x* and *y* reference axes indicated in Fig. 4 correspond to the axes in Fig. 5 and the plate numbering system with reference to these axes is shown in Fig. 3. Fig. 5 shows that the plate reorganization illustrated in Fig. 4 is not unique, numerous reorganizations have occurred during this calculation. During the 0.027 time units shown, the plates have changed direction by 630° (or seven changes of 90°). Fig. 5 also indicates that changes in direction occur almost continuously over some periods (for example, from 0.0054 to 0.0162) while they may punctuate relatively steady stages at other times. (For example, the change in direction shown in Fig. 4 follows a relatively steady stage.) Also note that the first six changes in direction of each plate are all in the same direction, only the final change is in a direction opposite to the previous changes.

In Fig. 6 we show a snapshot from a calculation that is identical to the calculation presented in Fig. 4 except that a depth-dependent viscosity profile is now specified. We refer to this calculation as model 3D2 in the text below. We find that the increase in viscosity in the lower mantle results in a steady-state flow. Flow reorganization is absent. This result is consistent with the findings of the 2-D study. However, in the 3-D calculation, plate motion is not required to be orthogonal to the plate boundaries and this extra degree of freedom allows plate spreading that is oblique to the divergent boundaries in the final steady solution of model 3D2.

The 2-D study indicates that flow reversals reappear when the introduction of the depth-dependent viscosity is accompanied by a Rayleigh number increase (Fig. 1). Accordingly, we tested the effect of the heating mode in a 3-D geometry to see whether plate reorganizations appear for the same heating mode where plate reversals were present in 2-D calculations.
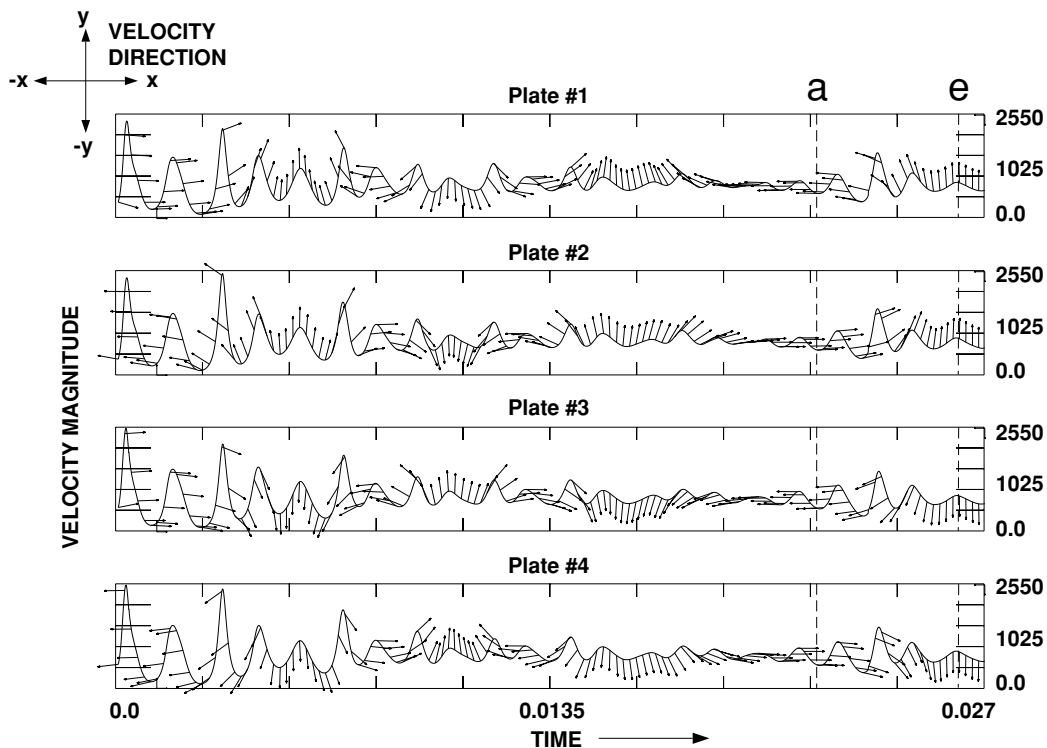
Figure 5. Model 3D1: the plate velocity magnitude as a function of time for the four plates in model 3D1. Also shown on the plots by fixed length arrows in the plane of the page, is the direction that each plate is moving in the *x–y* coordinate system shown in the figure. The *x–y* axes orientation corresponds to the *x–y* axes shown in Figs 3 and 4. Times corresponding to the frames in Figs 4(a) and (e) are marked by vertical dashed lines.
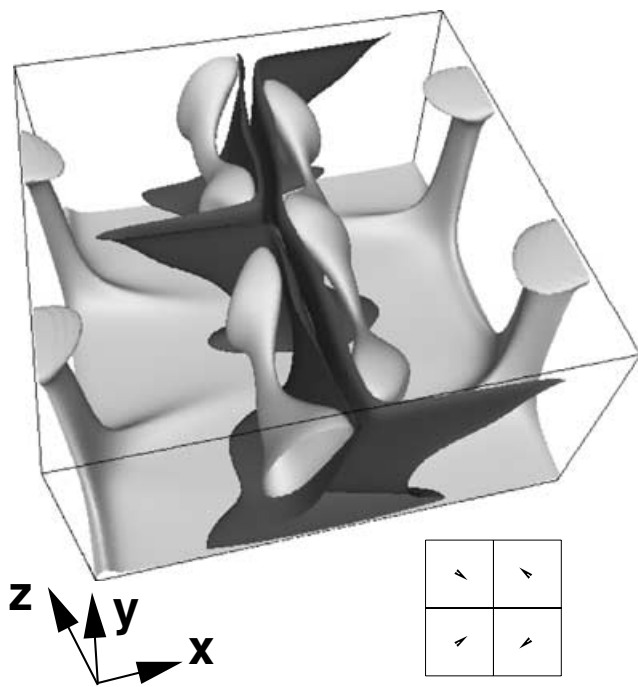
Figure 6. Model 3D2: snapshot of isosurfaces of constant temperature from a $2 \times 2 \times 1$ Cartesian geometry model with four square (equal in size) plates. The plate geometry for the calculation is also shown with the plate velocity direction indicated by arrows. the plate velocity direction indicated by arrows. The plate velocity magnitude is indicated by the arrow length. The calculation has a depth-dependent viscosity that increases with depth below the plates (see the text for further details). The Rayleigh number, Ra_B, is 5×10^6, and the rate of internal heating is 15. The plates have a thickness of $0.047d$ and a viscosity that is 1000 times greater than the fluid at their base. The light coloured isosurface corresponds to a temperature, T, of 0.91. The dark isosurface corresponds to a temperature of 0.61 and is shown only for depths greater than $0.078d$. The mean temperature of the model is 0.76. The solution has reached a time-independent steady state. The calculation resolution is $216 \times 216 \times 128$.

Fig. 7 shows a sequence of temperature fields from a 3-D calculation with a depth-dependent viscosity profile, a Bénard–Rayleigh number of 5×10^8 and $H = 15$ (model 3D3). Plate velocities are indicated at each time as in Fig. 4. This heating mode and viscosity structure is exactly the same as in the 2-D calculation shown in Fig. 2. The plate geometry is the same as in models 3D1 and 3D2. During the sequence shown, each plate has rotated by approximately $90°$. The flow under each plate in model 3D3 is not as similar as the flow under each plate in the 2-D calculation (Fig. 2); however, similarly to model 3D1, model 3D3 has evolved to a flow with strong symmetry. As was the case in the isoviscous calculation, we find that the plate reorganizations in the depth-dependent viscosity calculation occur quite gradually. Perhaps as a result, the period between reorganization stages is not particularly long. Because the plate reorganization is slow, new regions in the fluid interior start to become anomalously warm adjacent to newly formed downwelling sheets before a $90°$ change in plate direction has completed. The buoyancy associated with these regions precipitates yet another flow reorganization so that a cycle of almost continuous plate rotation develops.

The results described for model 3D3 were unaffected when we increased the aspect ratio of the calculation to $3 \times 3 \times 1$ (model 3D4).
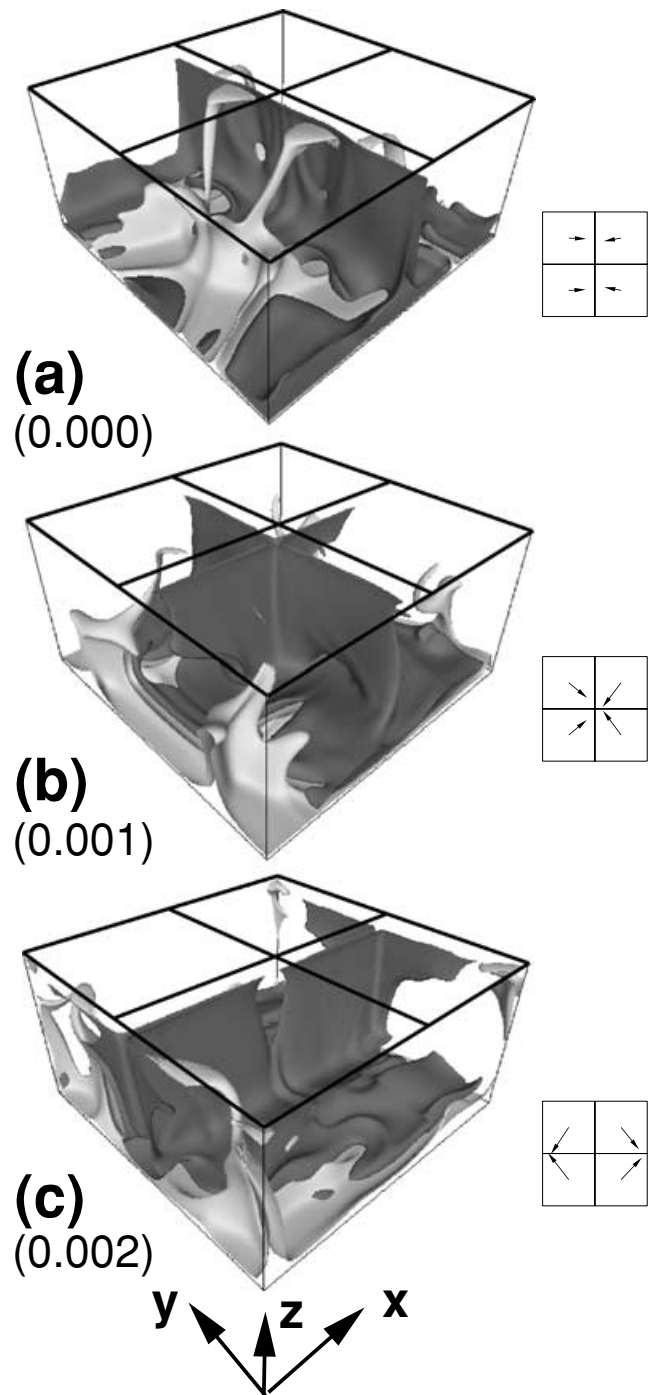
Figure 7. Model 3D3: a sequence of temperature field isosurfaces from a 3-D calculation in a $2 \times 2 \times 1$ geometry with four equal size square plates (each 1×1). Each temperature field plot is accompanied by a figure of the plate geometry for the calculation showing the corresponding plate velocity direction. The plate velocity magnitude is indicated by the arrow length. The Rayleigh number, Ra_B, is 5×10^7, the rate of internal heating is 15. The plates have a thickness of $0.047d$ and a viscosity that is 1000 times greater than the isoviscous fluid at their base. The time that has elapsed between frame (a) and each subsequent frame is indicated in parentheses next to each plot. The light coloured isosurface corresponds to a temperature, T, of 0.91. The dark isosurface corresponds to a temperature of 0.71. The mean temperature of the calculation is 0.81. The calculation resolution is $216 \times 216 \times 128$.

We found that a calculation with the identical viscosity structure and heating mode as model 3D3 but four 1.5 × 1.5 plates exhibited continual episodes of plate revolution just as for model 3D3.

The initial conditions specified for each calculation were chosen randomly. Consequently, we observed calculations evolving through several initial, distinct, planforms. Models 3D1 and 3D3 evolve through very different planforms before settling into patterns characterized by convergent boundaries with a length of 2*d*. This observation suggests that the occurrence of reorganization events is not dependent on the initial flow adopting a particular initial convection pattern. Most relevant to the Earth is our finding that the observed time-dependent flow in the four square plate calculations is essentially continuous and *does not* appear to be separated by steady stages.

To determine the effect of the symmetry of the four square plate geometry on our findings we examined models with the isoviscous (model 3D5) and depth-dependent (model 3D6) viscosity profiles and the plate geometry illustrated in Fig. 3(b). In Fig. 8 we present a sequence of temperature isosurface plots from the depth-dependent viscosity calculation to illustrate the evolution of the flow during a sequence of rapid plate reorganization (model 3D6). The dark grey isosurface corresponds to a temperature of 0.65. The light grey isosurface corresponds to a temperature of 0.85. The mean temperature of the calculation during the sequence shown is approximately 0.75. The plate boundary locations are shown with thick black lines on top of the boxes and a reference coordinate system is shown below the figures. Plate velocities are also indicated at each time, as in Fig. 4.

In Fig. 8(a), a pair of cold downwelling sheets are sinking along two of the boundaries defining the extent of the large 1.5 × 1.5 plate (the plate closest to the viewer). Convergence is occurring along one boundary of the small square plate (the boundary parallel to the *y*-axis that is hidden from the viewer). The pull on the large plate resulting from entrainment of the upper-mantle flow toward the two long downwelling sheets results in the large plate exhibiting a velocity with similar magnitude components in the *y* and −*x* directions. In Fig. 8(b) a major plate reorganization event begins and the motion of the large plate becomes almost parallel to the *y*-axis as the downwelling flow parallel to the *y*-axis has waned. As the reorganization continues, convergence commences along the other plate boundary parallel to the *y*-axis, resulting in a downwelling sheet-like flow. By the end of the sequence (Fig. 8e) the large plate has rotated by roughly 135° and a downwelling sheet of length 2*d* has developed along a boundary initially characterized by spreading and transform motion behaviour. The smallest plate has continued to move in a direction roughly parallel to the −*x*-axis during the entire sequence and the two long narrow plates have rotated by roughly 90° and 180°.

The temperature isosurface plots in Fig. 8 reveal that during the entire plate reorganization event a plume-like structure is present below the largest plate. In fact, the calculation adopts a flow pattern characterized by upwelling flow below the large plate for most of its evolution; however, it should be emphasized that these plumes are relatively weak (0.85 isosurface in a layer with a mean temperature of 0.75).

In Fig. 9 we show two curves representing the trajectories that a pair of particles would take if they were initially placed at the centre of plate 1 in model 3D1 (see Fig. 3a) and plate 1 in model 3D6 (see Fig. 3b). The initial position of both particles is coordinate (0, 0) in this figure. Each trajectory illustrates the path that a particle would take as it travels along with the plate velocity and therefore indicates the direction of plate motion at different times. In reality, if the
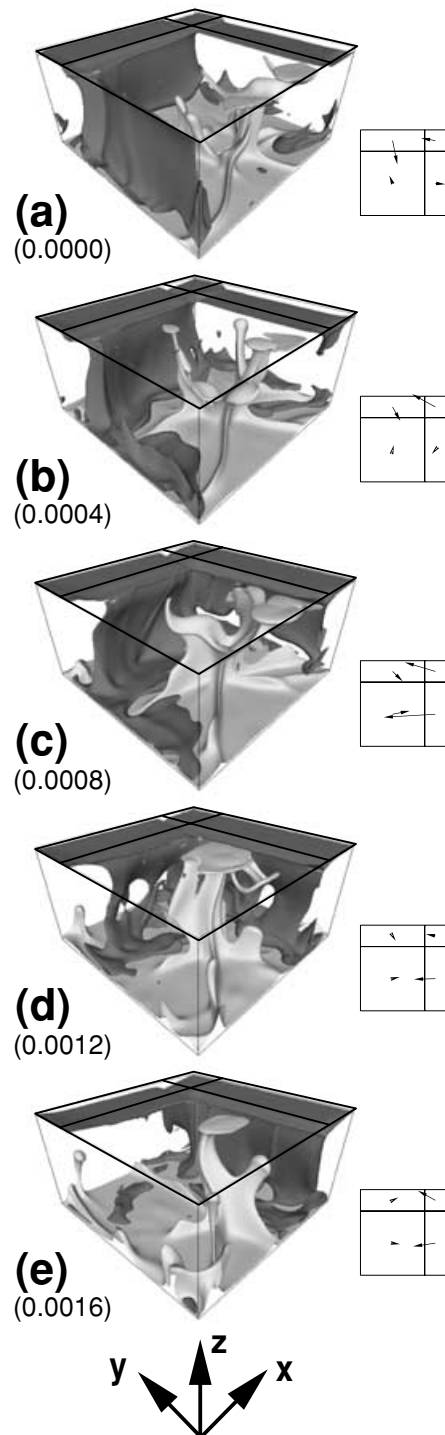
Figure 8. Model 3D6: a sequence of temperature field isosurfaces from a 3-D calculation in a 2 × 2 × 1 geometry with four rectangular plates (see Fig. 3b). Each temperature field plot is accompanied by a figure of the plate geometry for the calculation showing the corresponding plate velocity direction. The plate velocity magnitude is indicated by the arrow length. The Rayleigh number, Ra_B, is 5 × 10^7, the rate of internal heating is 15. The plates have a thickness of 0.047*d* and a viscosity that is 1000 times greater than the isoviscous fluid at their base. The time that has elapsed between frame (a) and each subsequent frame is indicated in parentheses next to each plot. The light coloured isosurface corresponds to a temperature, *T*, of 0.91. The dark isosurface corresponds to a temperature of 0.71. The mean temperature of the model is 0.81. The calculation resolution is 216 × 216 × 128.
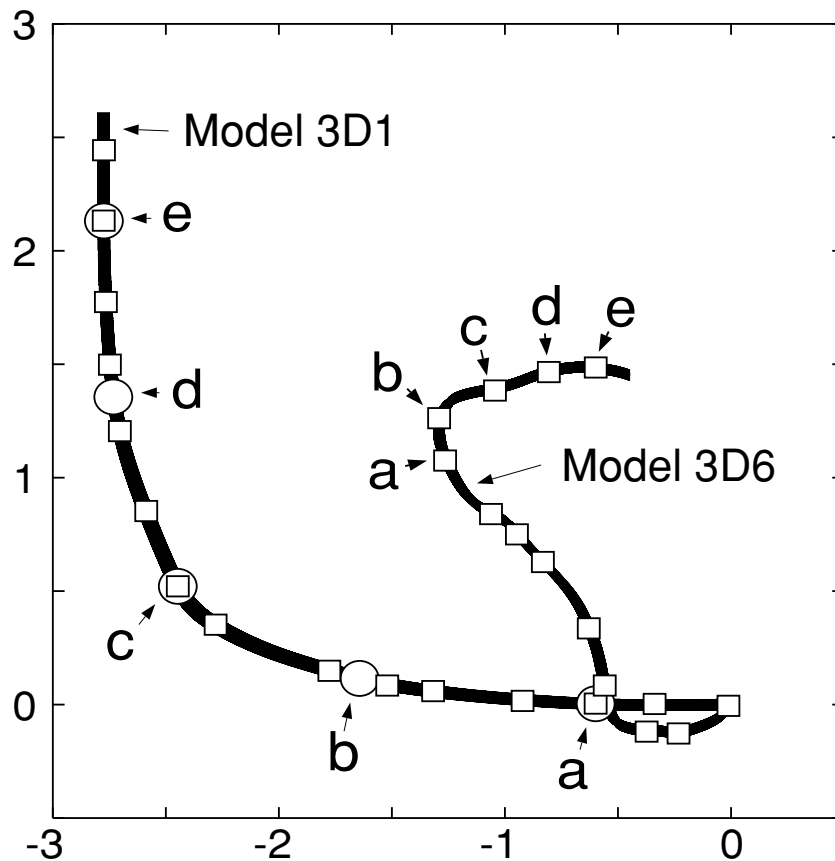
Figure 9. Trajectories (paths) of fictitious particles moving with the velocities of plates 1 (see Fig. 3) from the calculations illustrated in Figs 4 (model 3D1) and 8 (model 3D6). Squares mark each path at intervals separated by 0.0004 time units. Points labelled with an a correspond to the timing of frame (**a**) in Fig. 4 (model 3D1) and Fig. 8 (model 3D6). Additional labels, (**b**)–(**e**), correspond to the frames in the sequences shown in Figs 4 and 8 and indicate the position that each particle would have reached in the time corresponding to the temporal separation of the frames in Figs 4 (model 3D1) and 8 (model 3D6) relative to the position of the particles at the time of the corresponding frame (a).

particles were sitting on the plates they would reach a convergent plate boundary at some point and would subduct, so that the paths would terminate. However, we have continued to integrate the plate velocity time-series regardless of a particle reaching a plate boundary in order to show the direction of plate motion through time. The scales on the axes are units of non-dimensional distance and the squares marked along the paths are drawn at intervals of 0.0004 non-dimensional time units. The circles marked (a)–(e) indicate the times corresponding to the frames in Fig. 4. The times corresponding to frames (a)–(e) of Fig. 8 are also marked on the path for plate 1 of model 3D6. The paths indicate whether changes in plate direction have taken place gradually or rapidly by the sharpness of any changes in direction. In contrast to the path from model 3D1, the path from model 3D6 has sharp bends corresponding to changes in plate direction occurring over a short time. In addition, the total change in direction for the model 3D6 path is more than 180° (illustrated by the path initially leading in the negative *x*-direction and finally in the positive *x*-direction) during a period in which the change in direction of the plates in model 3D1 is less than 90°.

We find similar results for the isoviscous calculation with the same plate geometry as model 3D6 and conclude that removing the symmetry of the plate geometry from these systems results in a more time-dependent flow characterized by rapid changes in plate velocity.

4 DISCUSSION AND CONCLUSIONS

In a fluid layer confined between horizontal free-slip boundaries, the time dependence of the flow is affected by both the Bénard–Rayleigh number, Ra_B, and the internal heating rate, H. As the values characterizing whole mantle convection are approached, increasing either parameter (Ra_B or H) while the other remains fixed results in highly time-dependent flows featuring short-wavelength instabilities in the upper thermal boundary layers. In isoviscous systems, upwelling–downwelling separations of half the layer thickness and less are observed for mantle-like heating modes (e.g. Sotin & Labrosse 1999). We find that in 2-D free-slip surface calculations with depth-dependent viscosity, single upwellings are observed, but as flows become increasingly vigorous (i.e. the Rayleigh number is increased) numerous upper boundary layer drips are formed within a distance from the upwelling that is less than the layer thickness, *d*. Similar behaviour was observed in the 3-D flows described by Dubuffet *et al.* (2000).

The addition of plates to these convecting models fundamentally changes the character of the convective wavelength of the systems in comparison with the free-slip surface cases. Plates instill a wavelength on the flow that reflects the plate geometry. In addition, viscous plates suppress instabilities in the upper thermal boundary layers of the systems, curtailing the onset of time dependence (in

particular, this is true of the depth-dependent viscosity calculations with $Ra_B \leq 5 \times 10^6$). In the same heating mode regimes where 2-D free-slip surface convection dissolves from a flow with unit aspect ratio cells into narrow aspect ratio cell flow, convection with plates is characterized by dramatic changes in plate velocity. As Ra_B and H are both increased to Earth-like values, regular plate reversals are observed in 2-D calculations. In 3-D systems this behaviour is manifested as either continuous changes in plate direction (model 3D1, 3D3 and 3D4) or sudden changes in plate direction punctuating relatively steady stages (models 3D5 and 3D6). Behaviour of the latter type occurs when the plate geometry is non-symmetric—the case that is most applicable to the Earth.

A clear difference between the models presented here and plate evolution on the Earth is that plate boundaries in our models are static. Consequently, while plate motion in our models may adjust to reflect the distribution of buoyancy within the mantle, the plate geometry cannot. It cannot be ruled out that the stationarity of the plate boundaries could play some role in a build-up of heat in our calculations, either globally or locally, that would not exist in a system with evolving plate margins. However, it has been shown that the long-wavelength flow exhibited in convecting systems with plates is present in internally heated models that include migrating plate boundaries (Zhong & Gurnis 1993). Because it is the effect of the convective wavelength change that is responsible for the high temperatures and low heat flow observed in models with plates, we argue that the behaviour we describe that arises from the imposition of long-wavelength flow on internally heated convecting systems will probably remain present in a system with evolving plate boundaries. The influence of evolving plate boundaries on these systems should be the focus of a future study, however, the present study has allowed us to isolate the dynamics that evolve from the feedback between plate motion and internally heated 3-D convection and shows that episodic plate reorganization can occur without the complication of an evolving plate geometry.

Before comparing our calculations with the geological record, it is informative to summarize some of the general differences we have found between the results from 2-D and 3-D models. Unlike 3-D calculations, changes in plate direction in 2-D flows require that plate motion must cease, at least for an instant, because only $180°$ changes in direction are permitted. As a result, the surface heat flux is drastically reduced during episodes of plate reorganization. In contrast, Fig. 5 shows that plate velocities often increase at the onset of plate reorganizations in a 3-D flow. Heat flow in 3-D calculations is therefore not regularly retarded because of extreme drops in plate velocity. As a result, 2-D and 3-D plate calculations with the same heating mode have dissimilar mean temperatures. For example, the 3-D isoviscous calculation (model 3D1) depicted in Fig. 4 has a time-averaged mean temperature of approximately 0.80; almost 10 per cent cooler than the corresponding 2-D calculation that supplied the data point in Fig. 1. Contrasts in mean temperature between 2-D and 3-D depth-dependent viscosity calculations with plates show similar differences. Moreover, 3-D calculations appear slightly cooler than 2-D calculations, even in the absence of time-dependent flow. Model 3D2 (Fig. 6) has a time-averaged mean temperature of approximately 0.75, while the 2-D calculation with unit-width plates and the same heating mode has a mean temperature of 0.81.

Despite being cooler than their 2-D counterparts, the temperatures of the 3-D calculations are still greater than what might be expected for the mantle. There are at least two reasons why this might be the case. The first is a consequence of the Rayleigh number. Given a constant internal heating rate and an isothermal bottom boundary condition, the mean temperature becomes a decreasing function as

the Rayleigh number is increased. Sotin & Labrosse (1999) inverted the data from a suite of 3-D Cartesian-geometry, isoviscous, internally heated calculations with isothermal horizontal boundaries to yield an equation for the mean temperature of such a system as a function of Ra_B and H. Their findings indicate a decrease in temperature of almost 5 per cent when $H = 15$ and Ra_B is increased from 5×10^6 to 10^7. If this finding is applied to the plate-model calculations, a reduction in temperature of 5 per cent would still imply that a calculation with the plate geometry shown in Fig. 3(a), convecting with whole-mantle-type vigour ($Ra = 10^7$), could be expected to have a mean temperature of approximately 0.76. In contrast, the findings of Sotin & Labrosse (1999) predict that a free-slip surface calculation with $H = 15$ and $Ra_B = 10^7$ would have a mean temperature of 0.67. Thus, as is the case in 2-D convection, the effect of plates on 3-D convection is to increase the mean temperature. (Note that for the case that is the focus of this discussion, $Ra_B = 5 \times 10^6$ and $H = 15$, the difference in mean temperature between a 3-D free-slip surface calculation and the 3-D calculation with four unit-dimension square plates is only 11 per cent, whereas the difference in mean temperature between a 2-D free-slip surface calculation and a calculation with two unit-width plates is 36 per cent.) In both 2-D and 3-D calculations we can conclude that by instilling a wavelength on the convection that reflects their geometry, plates retain heat in the mantle relative to equivalent free-slip calculations. However, this phenomenon appears to be more dramatic in 2-D calculations because 3-D free-slip surface calculations are warmer than identically heated 2-D calculations (e.g. Parmentier *et al.* 1994) and because 3-D plate calculations are cooler than their 2-D counterparts.

In addition to the fact that a stiff lower mantle results in lower mean temperatures, the spherical geometry also has a significant effect on the temperature of the convecting medium. The effect of plates on the temperature profile in a spherical shell mantle was examined recently by Monnereau & Quéré (2001). These authors described a significant increase in mean temperature and a decrease in total heat flux in calculations with plates compared with calculations with free-slip boundaries. They also found that calculations with fewer plates are hotter than calculations with numerous smaller plates. In all cases they find that free-slip surface calculations are cooler than calculations with plates. However, though they do describe time-dependent calculations, these authors did not identify the potential role of plate reorganization in cooling the mantle. Nevertheless, the findings from the spherical geometry study support our conclusion that plates significantly elevate mantle temperatures by suppressing the most efficient convection patterns.

The evidence from the study presented here and Monnereau & Quéré's (2001) spherical geometry study cannot verify whether plate reorganization events will mantle convection with plates in a spherical shell to be cooled more efficiently at Earth-like Rayleigh numbers than Rayleigh numbers an order of magnitude lower. However, we suggest that the reorganization of plate velocities associated with the transition to convection at mantle-like vigour cools the mantle more efficiently than can be predicted by interpreting the results from 2-D or lower Rayleigh number 3-D calculations. Ultimately, 3-D spherical shell mantle convection calculations with plates and high Rayleigh numbers will be required to determine the importance of plate reorganization in cooling the mantle and how much cooler spherical geometry calculations with plates might be in comparison with Cartesian geometry calculations.

The effect of plates on mantle temperatures in these 3-D convection calculations is interesting, though perhaps predictable; however, the dramatic changes in plate velocity that accompany the introduction of plates could not be anticipated. We claim that it is

the influence of the plates on the temperature field of the internally heated mantle that is directly responsible for their unstable velocity patterns. The presence of the plates impedes heat flow to the surface and traps heat in the upper mantle. As the plates move, they entrain the mantle below and carry this trapped heat toward the sheet-like downwellings at convergent plate boundaries (the analogue of subduction zones in these calculations). Hot material that has reached the region below the oldest plate is entrained by the downwelling flow deep into the mantle where it envelops the cold downwelling sheet. Owing to its buoyancy, the hot upper-mantle material resists the downward drag of the downwelling flow and instead is trapped in a relatively stagnant region adjacent to the downwelling flow. In this region the buoyancy of the trapped hot material is balanced by the downward drag of the sinking cold sheet. The heat builds up in the regions around the downwellings and in time, the buoyancy associated with the heat overcomes the downwelling flow, perturbing the existing surface velocity pattern. This perturbation results in the onset of convergent flow along either a previously conservative or divergent plate boundary. The result of the development of the young convergent boundary is a rapid change in direction of plate motion driven by the combined effects of the push away from the old subduction zone, supplied by the buoyancy of the hot envelope, and the downward pull of the cold material sinking at the new convergent plate boundary.

The scenario described above requires hot material to build-up around the mature slab to set the plate reorganization event in motion. However, it is the negative buoyancy along a newly developing convergent boundary that takes over as the most significant contribution to the forces that drive plate motion in a new direction. Previous authors have suggested that changes in plate boundary forces are the catalysts responsible for plate reorganization events (e.g. Gordon *et al.* 1978); however, the dynamic plausibility of these hypotheses are difficult to test. One possible explanation for the change in direction of the Pacific plate was the development of a young subduction zone in the Western Pacific along the Izu–Bonin–Mariana island arc system (Stern & Bloomer 1992). If the pull from a slab associated with such a young subduction zone were responsible for the change in direction of the Pacific plate, the findings described herein would explain how the pull towards young subduction zones may supersede the pull from existing subduction zones, a condition that allows for more rapid changes in direction than might otherwise be expected. In the reorganization events exhibited in the calculations presented here, the pull towards mature slabs weakens prior to the onset of subduction along new convergent boundaries.

The general argument against mantle buoyancy forces as the mechanism driving short-timescale (<5 Myr) dramatic changes in plate velocity is that these forces evolve over many millions of years. Estimates for the change in direction of the Pacific plate are as short as 3 Myr. If the initiation of subduction in the western Pacific along an existing transform boundary was the key event in changing the direction of the Pacific plate it may have taken place approximately 5 Myr prior to the onset of the change in direction of the Pacific plate (e.g. Stern & Bloomer 1992). If such an event marked the beginning of the process that caused the Pacific Plate to change its spreading direction, then it implies a limit on the temporal separation between subduction initiation and the change in plate motion of no more than ~5 Myr. This rapid response has generally been used as an argument against the evolution of mantle buoyancy forces driving rapid changes in plate motion. However, in all of the calculations we have undertaken, we find that when new convergent plate boundaries form in response to the resistance of continued pull towards mature convergent boundaries, plate motion is very rapidly affected by the onset of subduction.

A measure of the timing of an event in one of our calculations can be attained as follows. If we take an event such as the change in direction of plate 1 in model 3D6 occurring between frames (a) and (c) of Fig. 9 as a typical example of plate reorganization in one of our non-symmetric calculations, we can estimate a dimensional time required for the almost 90° change in direction. The Rayleigh number of this calculation is a little low for the mantle, thus a dimensionalization using mantle parameters is not appropriate. (For example, we would find mean plate velocities of the order of 1.5 cm yr^{-1} using typical mantle parameters for model 3D6.) If we accept an appropriate average velocity for the plates of approximately 4 cm yr^{-1} and consider that a particle on the plate travels approximately $0.4d$ or 1200 km between frames (a) and (c) in Fig. 9, then we find that a dimensional estimate of the time that elapses during this period is approximately 30 Myr and most of the change in direction of the plate (over 60°) takes place in less than 5 Myr. We also find that an estimate of the mean time between reorganization events is in the 200–250 Myr range. This range is representative of the behaviour in several calculations that we have examined; however, factors such as the prescribed plate geometry or a spherical geometry may affect the timing of the events. Indeed, we have found at least one example of a geometry in which reorganization is entirely absent. In calculations with two congruent triangular plates, flow locks into a steady pattern. However, such contrived cases are the exception and are less applicable to the Earth's evolution than calculations with different sized plates.

Based on the dimensionalization of our results and the robust behaviour exhibited over a wide variety of calculations, we conclude that plate reorganization (rapid changes in plate velocity) may result from the feedback between plate motion and internally heated mantle convection. The systems described here suggest that substantial changes in plate motion may occur on timescales of less than 5 Myr following a build-up of thermal buoyancy around mature subduction zones. This buoyancy instigates a sequence of events leading to a rapid change in plate direction.

REFERENCES

Bunge, H.-P. & Richards, M.A., 1996. The origin of large scale structure in mantle convection: effects of plate motions and viscosity stratification, *Geophys. Res. Lett.,* **23,** 2987–2990.

Bunge, H.-P., Richards, M.A. & Baumgardner, J.R., 1996. Effect of depth-dependent viscosity on the planform of mantle convection, *Nature,* **379,** 436–438.

Bunge, H.-P., Richards, M.A. & Baumgardner, J.R., 1997. A sensitivity study of three-dimensional spherical mantle convection at 10^8 Rayleigh number: effects of depth-dependent viscosity, heating mode, and an endothermic phase change, *J. geophys. Res.,* **102**, 11 991–12 007.

Busse, F.H. *et al.*, 1993. 3D convection at infinite Prandtl number in Cartesian geometry—A benchmark comparison, *Geophys. astrophys. Fluid. Dyn.,* **75,** 39–59.

Chandrasekhar, S., 1961. *Hydrodynamic and Hydromagnetic Stability*, p. 654, Clarendon Press, Oxford.

Clague, D.A. & Dalrymple, G.B., 1987. Geologic evolution of the Hawaiian–Emperor volcanic chain, *US Geol. Surv. Prof. Pap.,* **1350,** 5–54.

Davies, G.F., 1988. Role of the lithosphere in mantle convection, *J. geophys. Res.,* **93,** 10 451–10 466.

Davies, G.F., 1989. Mantle convection with a dynamic plate: topography, heat flow and gravity anomalies, *Geophys. J.,* **98,** 461–464.

Dubuffet, F., Rabinowicz, M. & Monnereau, M., 2000. Multiple scales in mantle convection, *Earth planet. Sci. Lett.,* **178,** 351–366.

Engebretson, D.C., Cox, A. & Gordon, R.G., 1985. Relative motion between oceanic and continental plates in the Pacific basin, *Geol. Soc. Am. Spec. Pap.,* **206,** 1–59.

Forte, A.M. & Mitrovica, J.X., 1996. New inferences of mantle viscosity from joint inversion of long-wavelength mantle convection and postglacial rebound data, *Geophys. Res. Lett.,* **23,** 1147–1150.

Gable, C.W., O'Connell, R.J. & Travis, B.J., 1991. Convection in three dimensions with surface plates: generation of toroidal flow, *J. geophys. Res.,* **96,** 8391–8405.

Gordon, R.G., Cox, A. & Harter, C.E., 1978. Absolute motion of an individual plate estimated from its ridge and trench boundaries, *Nature,* **274,** 752–755.

Gurnis, M., 1989. A reassessment of the heat transport by variable viscosity convection with plates and lids, *Geophys. Res. Lett.,* **16,** 179–182.

Gurnis, M. & Davies, G.F., 1986. Numerical study of high Rayleigh number convection in a medium with depth-dependent viscosity, *Geophys. J. R. astr. Soc.,* **85,** 523–541.

Gurnis, M. & Zhong, S., 1991. Generation of long wavelength heterogeneity in the mantle by the dynamic interaction between plates and convection, *Geophys. Res. Lett.,* **18,** 581–584.

Hansen, U., Yuen, D.A., Kroening, S.E. & Larsen, T.B., 1993. Dynamical consequences of depth-dependent thermal expansivity and viscosity on mantle circulations and thermal structure, *Phys. Earth planet. Inter.,* **77,** 205–223.

Houseman, G., 1988. The dependence of convection planform on mode of heating, *Nature,* **332,** 346–349.

Jarvis, G.T., 1984. Time dependent convection in the Earth's mantle, *Phys. Earth planet. Inter.,* **36,** 305–327.

Jarvis, G.T. & Peltier, W.R., 1982. Mantle convection as a boundary layer phenomenon, *Geophys. J. R. astr. Soc.,* **68,** 385–424.

King, S.D. & Hager, B.H., 1990. The relationship between plate velocity and trench viscosity in Newtonian and power-law subduction calculations, *Geophys. Res. Lett.,* **17,** 2409–2412.

King, S.D., Gable, C.W. & Weinstein, S.A., 1992. Models of convection-driven tectonic plates: a comparison of methods and results, *Geophys. J. Int.,* **109,** 481–487.

Lowman, J.P., King, S.D. & Gable, C.W., 2001. The influence of tectonic plates on mantle convection patterns, temperature and heat flow, *Geophys. J. Int.,* **146,** 619–636.

Lux, R.A., Davies, G.F. & Thomas, J.H., 1979. Moving lithosphere plates and mantle convection, *Geophys. J. R. astr. Soc.,* **57,** 209–228.

McKenzie, D.P., Roberts, J.M. & Weiss, N.O., 1974. Convection in the Earth's mantle: towards a numerical simulation, *J. Fluid Mech.,* **62,** 465–538.

Monnereau, M. & Quéré, S., 2001. Spherical shell models of mantle convection with tectonic plates, *Earth planet. Sci. Lett.,* **184,** 575–587.

Parmentier, E.M., Sotin, C. & Travis, B.J., 1994. Turbulent 3-D thermal convection in an infinite Prandtl number, volumetrically heated fluid: implications for mantle dynamics, *Geophys. J. Int.,* **116,** 241–251.

Parmentier, E.M. & Turcotte, D.L., 1978. Two-dimensional mantle flow beneath a rigid accreting lithosphere, *Phys. Earth planet. Int.,* **17,** 281–289.

Patriat, P. & Achache, J., 1984. India–Asia collision chronology has implications for crustal shortening and driving mechanism of plates, *Nature,* **311,** 615–621.

Pysklywec, R.N. & Mitrovica, J.X., 1997. Mantle avalanches and the dynamic topography of continents, *Earth planet. Sci. Lett.,* **148,** 447–455.

Richards, M.A. & Lithgow-Bertelloni, C., 1996. Plate motion changes, the Hawaiian–Emperor bend, and the apparent success and failure of geodynamic models, *Earth planet. Sci. Lett.,* **137,** 19–27.

Sotin, C. & Labrosse, S., 1999. Three-dimensional thermal convection in an iso-viscous, infinite Prandtl number fluid heated from within and from below: applications to the transfer of heat through planetary mantles, *Phys. Earth planet. Inter.,* **112,** 171–190.

Stern, R.J. & Bloomer, S.H., 1992. Subduction zone infancy: examples from the Eocene Izu–Bonin–Mariana and Jurassic California arcs, *Bull. geol. Soc. Am.,* **104,** 1621–1636.

Stock, J.M. & Molnar, P., 1987. Revised history of the early Tertiary plate motion in the southwest Pacific, *Nature,* **325,** 495–499.

Tackley, P.J., 1998. Self-consistent generation of tectonic plates in three-dimensional mantle convection, *Earth planet. Sci. Lett.,* **157,** 9–22.

Tackley, P.J., 2000. Mantle convection and plate tectonics: toward an integrated physical and chemical theory, *Science,* **288,** 2002–2007.

Travis, B. & Olson, P., 1994. Convection with internal heat sources and thermal turbulence in the Earth's mantle, *Geophys. J. Int.,* **118,** 1–19.

Travis, B., Weinstein, S. & Olson, P., 1990. Three-dimensional convection planforms with internal heat generation, *Geophys. Res. Lett.,* **17,** 243–246.

Travis, B. *et al.*, 1991. A benchmark comparison of numerical methods for infinite Prandtl number thermal convection in two-dimensional Cartesian geometry, *Geophys. astrophys. Fluid Dyn.,* **55,** 137–160.

Trompert, R. & Hansen, U., 1998. Mantle convection simulations with rheologies that generate plate-like behaviour, *Nature,* **395,** 686–689.

Weinstein, S.A., Olson, P.L. & Yuen, D.A., 1989. Time-dependent large aspect-ratio thermal convection in the Earth's mantle, *Geophys. astrophys. Fluid Dyn.,* **47,** 157–197.

Zhong, S. & Gurnis, M., 1993. Dynamic feedback between a continentlike raft and thermal convection, *J. geophys. Res.,* **98,** 12 219–12 232.

Zhong, S., Zuber, M.T., Moresi, L. & Gurnis, M., 2000. Role of temperature-dependent viscosity and surface plates in spherical shell models of mantle convection, *J. geophys. Res.,* **105**, 11 063–11 082.